AGU PUBLICATIONS

JGR

Journal of Geophysical Research: Space Physics

RESEARCH ARTICLE
10.1002/2013JA019712

Key Points:
- Observations of LSWS in spatial domain and its characteristics
- Physical neutral ion coupling process behind the excitation of LSWS
- Seeding of R-T instability and equatorial plasma bubbles by LSWS

Correspondence to:
S. Tulasi Ram,
tulasi@iigs.iigm.res.in

Citation:
Tulasi Ram, S., M. Yamamoto, R. T. Tsunoda, H. D. Chau, T. L. Hoang, B. Damtie, M. Wassaie, C. Y. Yatini, T. Manik, and T. Tsugawa (2014), Characteristics of large-scale wave structure observed from African and Southeast Asian longitudinal sectors, *J. Geophys. Res. Space Physics*, *119*, doi:10.1002/2013JA019712.

Received 17 DEC 2013
Accepted 16 FEB 2014
Accepted article online 23 FEB 2014

Characteristics of large-scale wave structure observed from African and Southeast Asian longitudinal sectors

S. Tulasi Ram[1], M. Yamamoto[2], R. T. Tsunoda[3], H. D. Chau[4], T. L. Hoang[5], B. Damtie[6], M. Wassaie[6], C. Y. Yatini[7], T. Manik[7], and T. Tsugawa[8]

[1]Indian Institute of Geomagnetism, Navi Mumbai, India, [2]Research Institute of Sustainable Humanosphere, Kyoto University, Uji, Japan, [3]Center for Geospace Studies, SRI International, Menlo Park, California, USA, [4]Hanoi Institute of Geophysics, Vietnam Academy of Science and Technology, Hanoi, Vietnam, [5]Ho Chi Minh City Institute of Physics, Vietnam Academy of Science and Technology, Ho Chi Minh City, Vietnam, [6]Washera Geospace and Radar Science Laboratory, Bahir Dar University, Bahir Dar, Ethiopia, [7]Space Science Center, Indonesian National Institute of Aeronautics and Space, Bandung, Indonesia, [8]National Institute of Information and Communications Technology, Tokyo, Japan

Abstract The spatial large-scale wave structure (LSWS) at the base of *F* layer is the earliest manifestation of seed perturbation for Rayleigh-Taylor instability, hence, found to play a deterministic role in the development of Equatorial Plasma Bubbles (EPBs). Except for a few case studies, a comprehensive investigation has not been conducted on the characteristics of LSWS because of the complexity involved in detecting the LSWS, particularly, in spatial domain. In this scenario, a comprehensive study is carried out, for the first time, on the spatial and temporal characteristics of LSWS observed in spatial domain over African and Southeast Asian longitudinal sectors during the year 2011. The observations indicate that these wave structures can be detected a few degrees west of *E* region sunset terminator and found to grow significantly at longitudes past the sunset terminator. The phase fronts of these spatial structures are found to align with the geomagnetic field ($\vec{B}$) lines over a latitudinal belt for at least 5−6° (~500–600 km) centered on dip equator. The zonal wavelengths of these structures are found to vary from 100 to 700 km, which is consistent with the earlier reports, and the EPBs were consistently observed when the amplitudes of LSWS were grown to sufficient strengths. These results would provide better insights on the underlying physical processes involved in excitation of LSWS in terms of important roles being played by *E* region electrical loading and polarization electric fields induced via spatially varying dynamo current due to neutral wind perturbations associated with atmospheric gravity waves.

1. Introduction

The postsunset development of equatorial plasma bubbles (EPBs) and their morphological features during both quiet and disturbed periods have been extensively studied and a rich literature was published during the past seven decades. The gravitational Rayleigh-Taylor (R-T) instability is the basic driving mechanism for the development of EPBs near *F* region sunset at geomagnetic equator [*Dungey*, 1956]. These local density depleted regions rapidly grow upward to the topside ionosphere under the action of polarization electric fields, and meridionally elongate along the field lines. Several cascaded instability processes are responsible for the evolution of irregularities with wide spectrum of scale sizes ranging from several hundred kilometers to about 10 cm [*Haerendel*, 1973; *Kelley*, 1989; *Abdu*, 2001]. Once developed, these EPBs generally drift eastward with velocities ranging from 50 to 200 m/s [*Aarons et al*., 1980; *Bhattacharya et al*., 2001; *Rama Rao et al*., 2005]. Promising favorable conditions for the development of postsunset EPBs have been identified. The post sunset rise (PSSR) of equatorial *F* region height is an important factor that creates the most favorable conditions for EPBs by increasing the growth rate of R-T instability [*Fejer et al*., 1999; *Whalen*, 2002; *Tulasi Ram et al*., 2006, and references therein]. The close alignment of sunset terminator with magnetic meridian and the symmetry of the north-south hemispheric ion densities are the other favorable conditions for the development of EPBs [*Tsunoda*, 1985; *Maruyama*, 1988; *Mendillo et al*., 1992; *Lee et al*., 2005]. The morphology of EPBs such as nocturnal, seasonal, longitudinal, and solar activity variability of EPB occurrence was more or less explained in terms of the above mentioned conditions.

In addition to above factors, there is an additional random factor that impedes our attempts to develop the predictive capabilities of EPBs is the initial seed perturbation. The atmospheric gravity waves (AGWs) were

believed to provide the required initial seed for EPBs by locally modulating the bottom side *F* region plasma into a spatial wave structure of enhanced and depleted regions. This spatial wave structure in the bottomside ionosphere can initiate the R-T instability and the EPBs develop from the depleted electron density regions [*Dungey*, 1956; *Huang and Kelley*, 1996; *Kelley*, 2004]. *Rottger* [1973] from the transequatorial HF propagation experiment has reported that perturbed structures in the bottomside *F* layer were distributed quasiperiodically in longitude, with an average separation distance of ~380–450 km. This quasiperiodic distribution of path-like structures was interpreted as due to a spatial wave-like plasma density structure in east-west direction. Later, *Tsunoda and White* [1981] and *Tsunoda* [1981] observed a zonal wave-like structure at the bottomside ionosphere with wavelengths varying from 300 to 600 km using Advanced Research Project Agency (ARPA) Long-range Tracking and Identification Radar (ALTAIR) incoherent scatter radar. This zonal wave structure manifested as a quasiperiodic modulation in the height of isoelectron density contours in backscatter radar maps, which were termed as a large-scale wave structure (LSWS) by *Tsunoda and White* [1981] and *Tsunoda* [1981, 2005]. Further, they showed that the EPBs grow from the upwellings (or crests) of LSWS. Recent studies using backscatter radar maps, airglow, ionosondes, scintillation, and in situ satellite observations further confirmed that a large-scale spatial wave-like modulation of the bottomside equatorial *F* region was probably excited by the AGWs and responsible for the periodic spacing of ~ 150–600 km between the EPB structures [*Eccles*, 2004; *Rama Rao et al*., 2005; *Fukao et al*., 2006; *Abdu et al*., 2009; *Makela et al*., 2010].

Despite the increasing amount of evidence (from case studies) that the zonal LSWS provides the required seed and controls the development of EPBs, not much was known about the characteristics of LSWS due to lack of sufficient observations in spatial domain. A reason for the paucity in observations is the inability to observe the LSWS, directly in spatial domain, by the existing instruments (except a very few observations earlier by ALTAIR steerable incoherent scatter radar). However, the signatures of LSWS can be observed from ground-based ionosondes by means of "satellite" traces [*Abdu et al*., 1981; *Tsunoda*, 2008] and multireflected echoes (MREs) [*Tsunoda*, 2009; *Thampi et al*., 2012]. After the launch of C/NOFS (Communication/Navigation Outage Forecasting System) with onboard CERTO (Coherent Electromagnetic Radio Tomography) beacon transmitter in near equatorial (13° inclination) orbit, *Thampi et al*. [2009], *Tsunoda* [2010b], and *Tsunoda et al*. [2011] have demonstrated the LSWS and subsequent development of EPBs by measuring the total electron content (TEC) and scintillation from the CERTO beacon signals from C/NOFS. *Tulasi Ram et al*. [2012] have described the detailed methodology to derive the LSWS in spatial domain using ground-based reception of radio beacon signals from low-inclination low Earth-orbiting satellites, such as C/NOFS.

Therefore, with knowledge that the zonal LSWS provides the required initial seed and controls the development of EPBs, this paper mainly focuses on the characteristics of LSWS for better understanding on the underlying physics of these zonal wave structures. Using the method described in *Tulasi Ram et al*. [2012] to derive LSWS in spatial domain (briefly described in section 2), we report the results of a comprehensive study on the characteristics of LSWS and its relationship with EPBs using statistically significant number of observations over African and Southeast Asian longitudinal sectors during the year 2011.

2. Data and Methodology

The ground-based GNU radio beacon receiver (GRBR) systems [*Yamamoto*, 2008] at low latitudes of Southeast Asia and African longitudinal sectors were used to measure the spatial (zonal) variation of total electron content (TEC) from the C/NOFS-CERTO beacon transmissions at 150 and 400 MHz in near equatorial orbit. The geographic coordinates and dip latitudes of the stations considered in this study are listed in Table 1. The vertical TEC observations from low-inclination C/NOFS orbits were estimated using the method described in *Tulasi Ram et al*. [2012]. For low-inclination orbits, the horizontal variation in TEC along the direction of satellite flight is mainly associated with a longitudinal variation produced by changes in local time or solar zenith angle. Hence, to the first order, this method assumes TEC variation with horizontal distance (zonal direction for C/NOFS) is quasi-linear and solves the system of equations for the unknown initial offset by bisquare-weighted least squares fitting. This method has been validated and found to be consistent with the well-established two-station method [*Leitinger et al*., 1975] and ground-based ionosonde observations [*Tulasi*

Table 1. The Geographic Coordinates and Dip Latitudes of the Stations

Station No.	Station Name	Station Code	Geographic Latitude	Geographic Longitude	Dip Latitude
1	Nha Trang	NHA	12.27	109.20	5.24
2	Ho Chi Minh City	HCM	10.85	106.56	3.52
3	Bac Lieu	BCL	9.29	105.71	1.67
4	Kototabang (EAR site)	EAR	−0.20	100.32	−9.92
5	Pontianak	PTK	−0.00	109.36	−9.19
6	Bahirdar	BDU	11.56	37.38	3.93

Ram et al., 2012]. The spatial LSWS was extracted from the measured TEC by subtracting the background variation with scale sizes larger than 800 km. *Tulasi Ram et al*. [2012] provide more details on the method for estimating the vertical TEC and the derivation of LSWS from low-inclination C/NOFS orbits.

3. Results

3.1. LSWS Observed in TEC From Low-Inclination C/NOFS Orbits

From the low-latitude stations considered in this study, the C/NOFS passes with elevation angles greater than 20° are visible about 6 to 7 times each day, and for approximately 10 to 12 min during each pass. The line of sight TEC measured from C/NOFS-CERTO radio beacon transmissions were converted into vertical TEC assuming a mean ionospheric pierce point height of 350 km. Because of low-inclination (13°) orbit of C/NOFS, the variation in TEC along the direction of satellite pass is mainly due to the longitudinal variation with little contribution from the latitudinal variation. For example, the vertical TEC observed from Bac Lieu (BCL) on 8 March 2011 for seven successive C/NOFS orbits at different UT times were shown in Figure 1a. The horizontal axis gives the ionospheric pierce point (IPP) in longitude of the C/NOFS pass in geographic coordinates. It can be seen from this figure that the TEC exhibits only a small variation with IPP longitude for the C/NOFS passes at times from 0425 UT to 0934 UT. However, the C/NOFS pass at 1118 UT exhibits a large decrease in TEC from the longitude 95°E to 120°E. The local time corresponds to 1118 UT at these longitudes vary from 1730 LT to 1900 LT. The green and red vertical dotted lines indicate the longitudes corresponding to the *E* region (110 km) and *F* region (200 km) sunset terminators, respectively. That means, the west of green

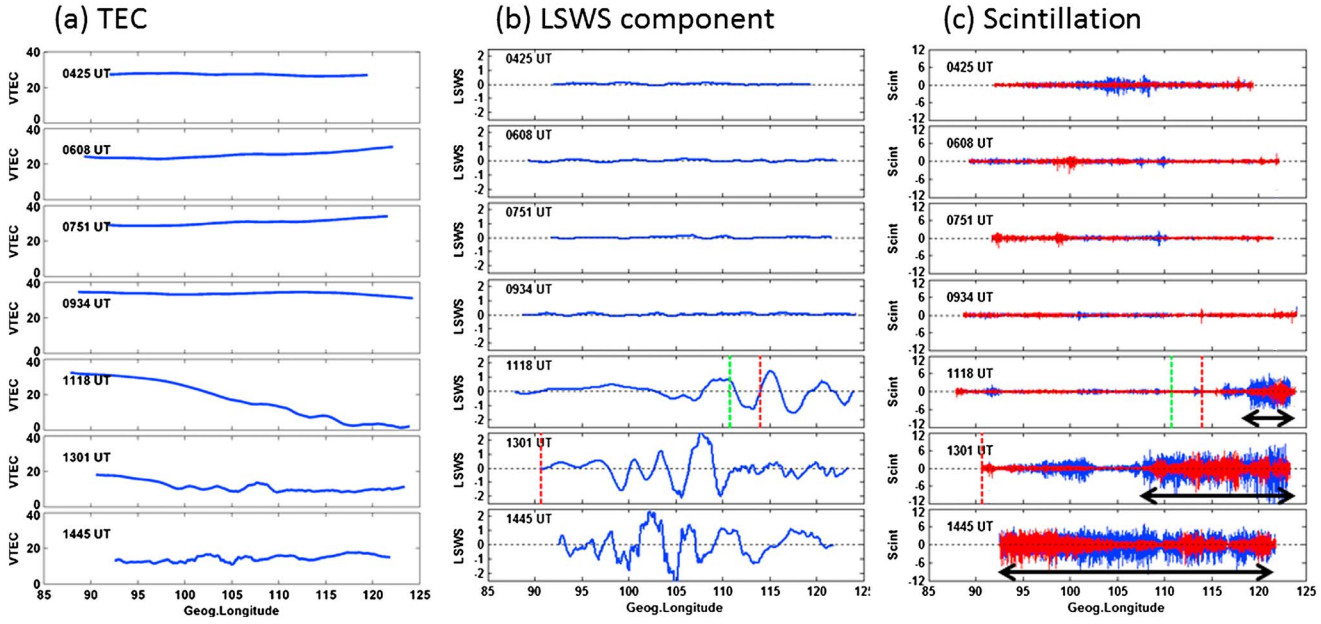

Figure 1. The spatial variations of (a) vertical TEC, (b) LSWS component, and (c) amplitude scintillation at 150 MHz (blue) and 400 MHz (red) observed from seven successive orbits of C/NOFS over Bac Lieu on 8 March 2011. The horizontal axis indicates the ionospheric pierce point (IPP) longitude of C/NOFS in geographic coordinates. The green and red vertical dotted lines (Figures 1b and 1c) indicate the locations of *E* region and *F* region sunset terminators, respectively. The double-headed arrows in Figure 1c indicate the amplitude scintillations at both 150 MHz and 400 MHz frequencies due to the presence of EPBs.

dotted line is the productive sunlit region, whereas the east of red dotted line is the recombinative dark region of ionosphere. Thus, the large gradient in TEC from sunlit to dark region of ionosphere (across the sunset terminator) is evident from the 1118 UT pass.

Another important observation from the C/NOFS pass at 1118 UT (also from 1301 UT pass) is that a spatial wave-like structure superimposed on the large background TEC gradient, which can be regarded as LSWS. Earlier reports by *Rottger* [1973], *Tsunoda and White* [1981], and *Makela et al*. [2010] indicate that the zonal wave lengths of LSWS excited by the atmospheric gravity waves may vary between 150 and 600 km. Therefore, the variations in TEC with zonal scale sizes greater than 800 km are assumed as background variation and subtracted from the longitudinal TEC variation in order to extract the LSWS component [*Tulasi Ram et al*., 2012]. The running average curve corresponding to 800 km spatial distance is computed by applying the hamming window weighting function [*Oppenheim and Schafer*, 1989] on the data series in both forward and reverse directions by adjusting the initial conditions to match with the DC component of the signal to get zero-phase distortion. This procedure is adopted to minimize the edge effects and the resultant running average curve has the same length of the original data series which is subtracted from the longitudinal TEC variation in order to extract the LSWS component. For example, Figure 1b illustrates the LSWS component after subtracting the background TEC variation for the same C/NOFS passes shown in Figure 1a. It can be seen from the Figure 1b that the LSWS component is almost zero for the daytime C/NOFS passes at times from 0425 UT to 0934 UT. However, the C/NOFS pass at 1118 UT exhibits significant wave-like structure (LSWS component) to the east of ~103°E longitude. The most interesting observation from this Figure 1b is that the LSWS component appears to be enhanced even in the sunlit region for just few degrees west of *E* region sunset terminator. Further, the amplitude of LSWS component appears to grow from sunlit to dark region of ionosphere across the sunset terminator similar to the observations of *Tsunoda* [2010b] and *Tsunoda et al*. [2013].

The subsequent development of EPBs and scintillation during that night can be observed (Figure 1c) at 150 MHz (blue) and 400 MHz (red) frequencies transmitted from C/NOFS-CERTO for the same passes shown in Figures 1a and 1b. It should be mentioned here that the EPBs would also manifest as depletion in measured TEC. Hence, sufficient care must be taken to distinguish between LSWS component and EPB induced depletions in TEC. In this context, the amplitude scintillations observed at 150 MHz and 400 MHz can be considered as an indication for presence of EPBs. The TEC measured around the longitudes where the significant amplitude scintillations at both 150 MHz and 400 MHz were observed (as marked by double-headed arrow in Figure 1c) is considered as plasma depletion due to presence of EPBs; hence, it cannot be considered as LSWS component. However, the wave-like structure between ~103°E and 117°E longitudes in Figure 1b can be considered as the LSWS component as there were no scintillations observed (no EPBs were present) at these longitudes. Therefore, in the rest of our analysis, the LSWS at those longitudes without any scintillation were only considered to study the characteristics of LSWS.

Figure 2 shows some examples of LSWS observed on a day-by-day basis for six successive days from Bahir Dar (African longitudes) and Bac Lieu (Asian longitudes) during March 2011. Figure 2 (left and right) corresponds to African and Asian longitudes, respectively. The green and red vertical dotted lines indicate the *E* and *F* region sunset terminators, respectively. The red double-headed arrows in each panel indicate the location of EPBs as observed from scintillations at both 150 and 400 MHz frequencies. It can be consistently observed from this figure that the peak-to-peak amplitude of LSWS grows from sunlit to dark region of ionosphere across the sunset terminator(s) at both longitudinal sectors on almost all days except on 10 March. Another interesting observation is that the peak-to-peak amplitude of LSWS component starts growing even in the sunlit region from few degrees west of *E* region sunset terminators on most of the days (for example, on 7–9 March over Bac Lieu and on 6–9 March over Bahir Dar). On the other hand, there was no significant LSWS component observed on 10 March over both the longitudinal sectors. Further, no scintillations were observed from C/NOFS overpass at 1146 UT and the next two successive C/NOFS passes over Bac Lieu during that night (10 March). The absence of Spread *F* on that night is further confirmed from the colocated ionosonde observations at Bac Lieu (not shown in figure) operated under Southeast Asia Low-latitude Ionospheric Network (http://wdc.nict.go.jp/IONO2/SEALION/index.html). The C/NOFS passes at 1637 UT (shown in Figure 2) and 1821 UT of 10 March over Bahir Dar also did not exhibit any scintillations indicating the absence of EPBs over African (20°–55°E) longitudinal sector during that night.

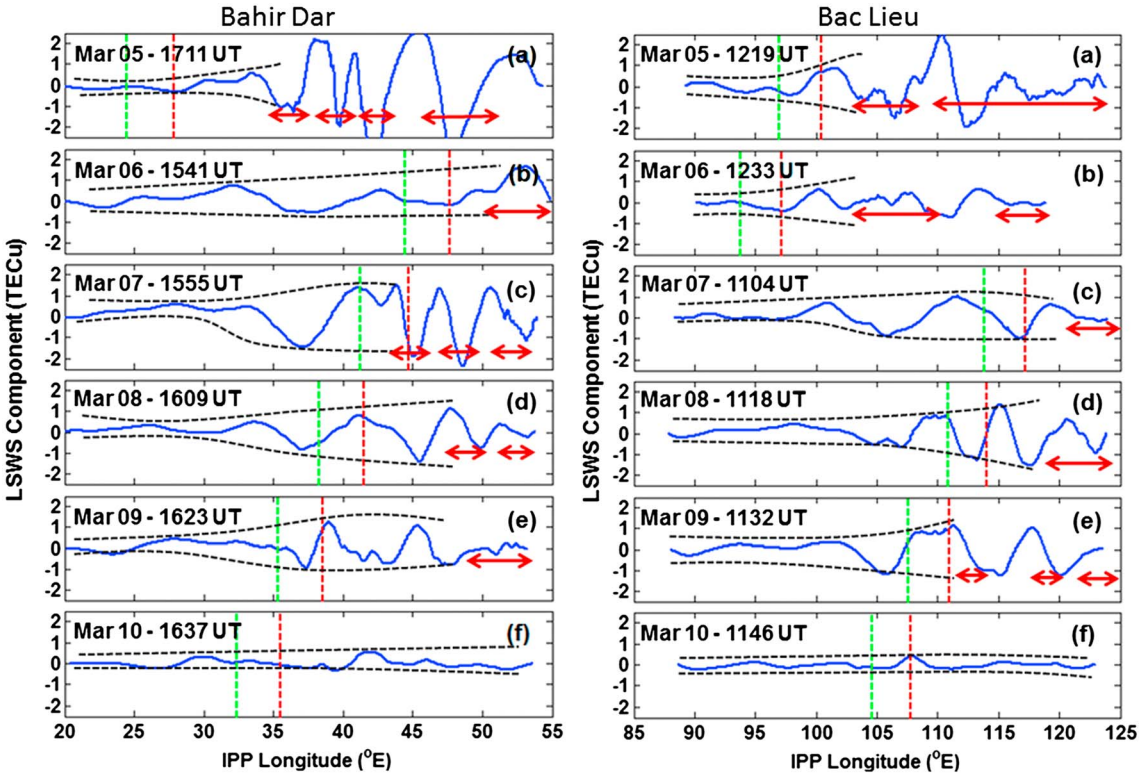

Figure 2. The LSWS observed on day-by-day basis for six successive days over Bahir Dar (African sector) and Bac Lieu (Asian sector) during March 2011. The green and red vertical dotted lines indicate the locations of *E* and *F* region sunset terminators, respectively. The red (horizontal) double-headed arrows in each panel indicate the location of EPBs from scintillation observations at 150 and 400 MHz frequencies. The broken lines in each panel are drawn at bottom and top of LSWS component by joining the negative and positive peaks of LSWS component, respectively (for better illustration purpose only).

3.2. Field Line Alignment of LSWS Phase Fronts

Figure 3 shows the simultaneous observations of LSWS observed from five low-latitude stations that are spatially distributed over Southeast Asian region on three typical days. In this figure, the observations from Bac Lieu (BCL), Ho Chi Minh City (HCM), Nha Trang (NHA), Kototabang (EAR), and Pontianak (PTK) were shown in blue, red, green, pink, and black colors, respectively. In Figures 3a, 3c, and 3e, the locations of the stations and ionospheric pierce point (IPP) trajectories of C/NOFS passes as observed from the respective stations were shown in geographic coordinates. Figures 3b, 3d, and 3f show the LSWS component observed from these stations in respective colors. The green and red vertical dotted lines indicate the location of *E* and *F* region sunset terminators, respectively. The double-headed arrows in Figures 3b, 3d, and 3f indicate the longitudes where scintillations were observed at both 150 MHz and 400 MHz frequencies; hence, they are considered as depletions due to EPBs. The black rectangles indicate the longitudes of interest where the LSWS component is observed that is free from presence of EPBs. It can be seen from this figure that the LSWS observed from BCL and HCM/NHA is always spatially aligned due to close proximity of their IPP trajectories. However, the most interesting observation is that the LSWS observed from the stations which are separated by large distances and located on either side of the dip equator were also spatially aligned. For example, from Figures 3a and 3b, the LSWS component observed from BCL, HCM, NHA, and EAR were spatially aligned around 92–110°E longitudes where their IPP trajectories were separated by 5–6° latitudes (~ 500–600 km) and are located on either side of the dip equator. Similar spatial alignment of LSWS can consistently be observed on other days shown in Figures 3d and 3f. It is further interesting to note that the alignment of LSWS can even be observed at longitudes that are few degrees west of *E* region sunset terminator (sunlit region). However, at longitudes much before the *E* region sunset terminator, the alignment is not clearly seen and the amplitudes of LSWS are smaller. This spatial alignment of LSWS over a wide latitudinal belt of 5–6° (~500–600 km) centered around dip equator suggests that the phase fronts of these zonal structures are aligned to geomagnetic field (*B*) lines as the declination angle of field lines in this sector is nearly zero.

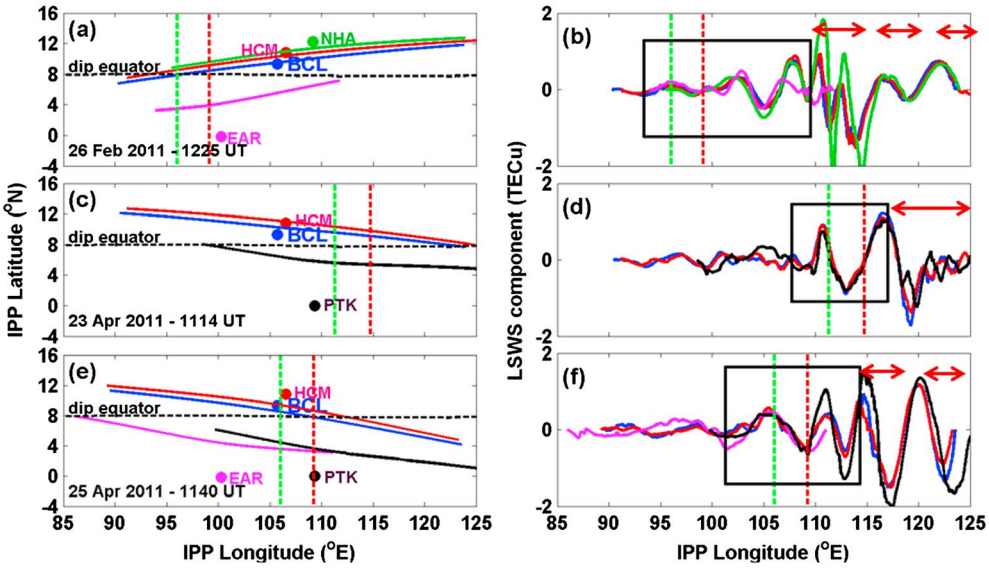

Figure 3. Simultaneous observations of LSWS from five low-latitude stations that are spatially distributed over Southeast Asian region. (a, c, e) The locations of stations and IPP trajectories of C/NOFS passes as observed from respective stations (in respective colors) in geographic coordinates. (b, d, f) The LSWS component observed from these stations in respective colors. The green and red vertical dotted lines indicate the locations of *E* and *F* region sunset terminators, respectively. The red (horizontal) double-headed arrows in each panel indicate the location of EPBs from scintillation observations at 150 and 400 MHz frequencies.

3.3. Zonal Wavelengths of LSWS

With a view to further examine the zonal wavelengths, the horizontal zonal distance between the two successive peaks of LSWS component were computed from the observations over Bahir Dar and Bac Lieu corresponding to African and Asian longitudinal sectors, respectively. Because of close proximity between the stations Bac Lieu and Ho Chi Minh City, the observations from Ho Chi Minh City were considered on some occasions when the data from "Bac Lieu" are not available while calculating the statistical results that presented in Figures 4–6. For example, Figures 4a and 4b show the histograms of zonal wavelengths of LSWS over African (20–55°E) and Asian (85–125°E) longitudinal sectors during the year 2011. It can be seen from this figure that the histogram of zonal wavelengths at both longitudinal sectors is similar, and the zonal wavelengths vary mostly between 100 and 700 km with a maximum around 200–500 km. These results are quite consistent with the earlier reports using different observation techniques such as transionospheric HF propagation experiment, steerable incoherent scatter radar, satellite in situ, ionosonde, and airglow observations by *Rottger* [1973], *Tsunoda and White* [1981], *Singh et al.* [1997], *Abdu* et al. [2009], and *Makela et al.* [2010], respectively. The zonal wavelengths of LSWS component obtained in this analysis were limited to less than 800 km as the spatial scale sizes greater than 800 km are assumed as the background variation and subtracted from the TEC variation (section 3.1).

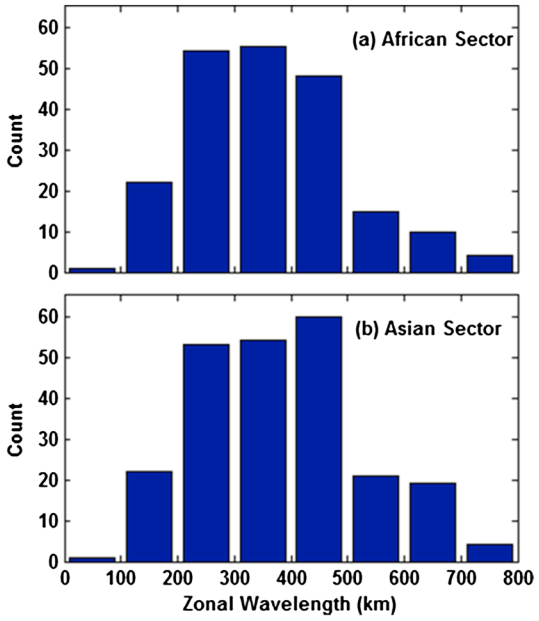

Figure 4. The distribution of zonal wavelengths of LSWS observed over (a) African (20–55°E) and (b) Asian (85–125°E) longitudinal sectors during the year 2011.

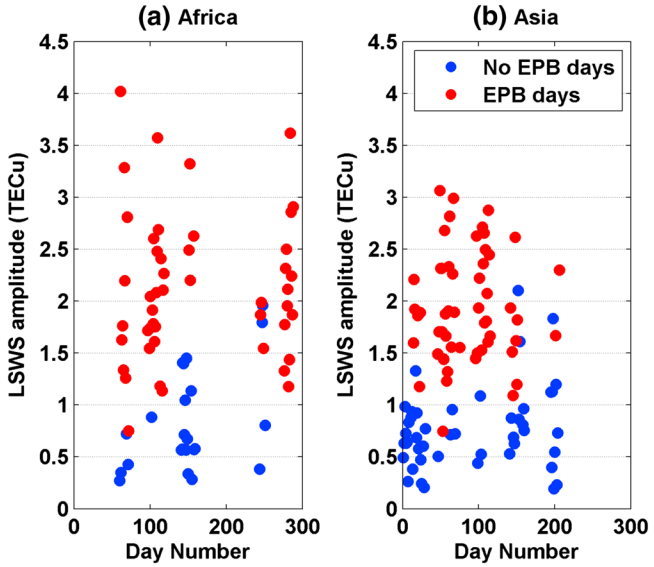

Figure 5. Day-by-day variations of LSWS amplitudes over (a) African (20–55°E) and (b) Asian (85–125°E) longitudinal sectors during the year 2011. The red/blue color dots indicate the days when the EPBs were present/absent over that longitudinal sector, respectively.

3.4. LSWS Amplitude and EPB Occurrence

It was shown that the zonal LSWS provides the required initial seed perturbation, and the EPBs would grow from the upwellings or crests of the LSWS [*Tsunoda and White*, 1981; *Tsunoda*, 1981, 2005; *Tsunoda et al.*, 2011; *Tulasi Ram et al.*, 2012]. In order to further understand the strength of LSWS and its influence on the development of EPBs, the peak-to-peak amplitude of LSWS is estimated from 70 days of observations over Bahir Dar and 99 days of observations over Bac Lieu during 2011. Here the peak-to-peak amplitude of LSWS as taken as the absolute difference between the peak of upwellings and the peak downwellings in the LSWS component observed on a given day. Figures 5a and 5b show the daily variation of LSWS amplitudes over African (20–55°E) and Asian (85–125°E) longitudinal sectors. The horizontal axis shows the day number in the year 2011, and the vertical axis indicates the LSWS amplitude in TEC units. The scintillations observed at both 150 MHz and 400 MHz frequencies from the C/NOFS passes during postsunset hours to midnight were used to determine the presence/absence of EPBs over the respective longitudinal sectors. The red/blue color indicates the days when the EPBs were present/absent over that longitudinal sector, respectively. It can be clearly seen from this figure that EPBs were present at both the longitudinal sectors on almost all the nights when the amplitude of LSWS grows sufficiently high, i.e., above 2 TEC units. On the other hand, the EPBs were absent during most of the nights (except three cases in African and one case in Asian sectors) when the amplitude of LSWS is less than 1 TEC unit. An interesting difference

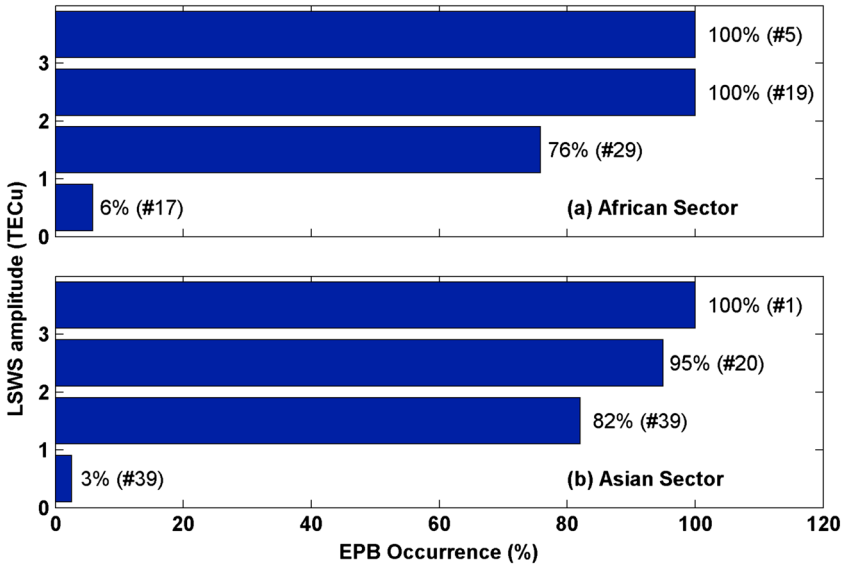

Figure 6. The percentage of EPB occurrence over (a) African (20–55°E) and (b) Asian (85–125°E) longitudinal sectors as a function of LSWS amplitude. The numbers shown in brackets indicate the total number of observations in that respective interval.

between African and Asian sectors that can be observed from Figure 5 is that the amplitudes of LSWS over African sector are slightly higher than Asian sector. For example, the LSWS amplitudes over African longitudes often grew to more than 3 TEC units (Figure 5a), whereas the LSWS over Asian longitudes (Figure 5b) are mostly less than 3 TEC units.

Figures 6a and 6b show the EPB occurrence (%) over African (20–55°E) and Asian (85–125°E) longitudes as a function of LSWS amplitude. It can be seen from this figure that the probability of EPB occurrence is very low when the peak-to-peak amplitude of LSWS is less than 1 TEC unit. However, the percentage of EPB occurrence increases quite significantly on the days when the amplitude of LSWS grows above 2 TEC units and becomes almost 100% when the LSWS amplitude is more than 3 TEC units at both the longitudinal sectors. The results from Figures 5 and 6 clearly indicate that the spatial LSWS provides the necessary seed and EPBs will develop when these spatial structures grown to sufficient strengths.

4. Discussion

The LSWS is spatial wave-like structure in the bottomside *F* layer, which is believed to be excited by the atmospheric gravity waves (AGWs) from the lower atmosphere. *Tsunoda* [2010c, 2012] has provided a theoretical explanation for the development of LSWS in terms of neutral-ion coupling. In a plane transverse to geomagnetic field lines ($\vec{B}$), the neutral wind perturbations ($\vec{u}$) associated with AGW induces a spatially varying dynamo current. For simplicity, consider a horizontally propagating AGW with a wave vector ($\vec{k}$) directed eastward and the associated neutral wind perturbations ($\vec{u}_z$) are in vertical plane transverse to the wave vector. The upward and downward wind perturbations ($\vec{u}_z$) induces a spatially oscillating Pedersen current, $\vec{j}_P = {}_P\left(\vec{u}_z \, X \, \vec{B}\right)$ in the direction of $\vec{k}$, where ${}_P$ is the Pedersen conductivity. In order to maintain current continuity, the polarization electric fields (E_P) would setup as given by [*Tsunoda* 2010c]

$$E_P = -\frac{\bar{u}_z \, B}{1 + \Sigma_P^E / \Sigma_P^F} \tag{1}$$

where Σ_P is field line-integrated Pedersen conductivity (with superscripts to indicate *E* or *F* layer) and $\bar{u}_z$ is the net u_z after integration. The vertical (upward/downward) transport of plasma due to these induced polarization electric fields (eastward/westward) causes a spatial wave-like modulation (upwelling/downwelling) of plasma in the bottomside equatorial *F* layer (LSWS) and the EPBs were found to evolve from the upwellings of LSWS [*Tsunoda and White*, 1981]. The important observations by *Tsunoda* [2010a] and *Tsunoda et al.* [2010] indicate that the seeding by LSWS can occur even when the postsunset rise of *F* layer (PSSR) is weak (during solstices) or completely absent (during very low solar activity).

The equation (1) indicates the role being played by *E* region conductivity (Σ_P^E) is crucial. The results presented in Figures 1 and 2 support this argument. The LSWS cannot grow during daytime due to the electrical loading by the *E* layer where the Σ_P^E is significantly large. However, the development of LSWS should be possible at longitudes few degrees west of sunset terminator (Figure 1b) where the *E* region loading is reduced due to higher solar zenith angles. At longitudes past the sunset terminator, the E_P response would improve with further decay of Σ_P^E and the amplitude of LSWS grow significantly. The finding of growing LSWS amplitudes from sunlit to dark region of ionosphere across the sunset terminator (Figures 1b and 2) is consistent with the E_P response. Further at postsunset longitudes, the additional eastward electric field by prereversal enhancement would augment the amplification of LSWS via R-T instability [*Tsunoda*, 2010c].

Generally for an isotropically launched AGW, the wave number has both components parallel ($k_{||}$) and perpendicular ($k_{\perp}$) to field lines. For the gravity wave component perpendicular to field lines, the plasma displacement (via $\vec{u}_z \, X \, \vec{B}$) is perpendicular to $\vec{B}$ and thus sets up periodic polarization charges (E_P) with alternative polarities separated by half wavelength distance along $k_{\perp}$. In contrast, for gravity wave component parallel to field lines, the E_P changes its polarity after each half wavelength distance along the direction of field line. Since the magnetic field line link cancels the alternative regions of positive and negative charges, the net E_P due to $k_{||}$ is negligibly small [*Klostermeyer*, 1978]. Therefore, the seeding (transfer of energy from neutral wind perturbations associated with AGW to the plasma) becomes optimum when the gravity wave propagates perpendicular to the $\vec{B}$ lines, and that phase fronts of AGW are aligned with $\vec{B}$ lines [*Klostermeyer*,

1978; *Huang and Kelley*, 1996; *Tsunoda*, 2010a, 2010c; *Tsunoda et al*., 2011]. The $\vec{B}$ line alignment of LSWS observed (Figure 3) over a wide latitudinal belt of 5–6° (~500–600 km) centered on dip equator provides the required observational evidence of this theoretical hypothesis. Once the seeding of R-T instability occurs via LSWS, the instability grows and amplifies the induced perturbations, and the EPBs would evolve from the upwellings of LSWS [*Tulasi Ram et al*., 2012; *Tsunoda et al*., 2011].

It is logical to argue that the periodic spacing between the EPBs echoes the horizontal wavelengths of AGWs that causes the excitation of LSWS. From the SpreadFEx campaign over Brazilian longitudes, *Takahashi et al*. [2009] have shown a linear relationship between the horizontal wavelengths of AGWs in the mesosphere and the spacing between successive EPBs. Using 630.0 nm airglow observations, *Makela et al*. [2010] have shown that the periodic spacing between EPBs observed over 123 clear nights (during 2006–2008) matches well with the spectrum of secondary gravity waves measured by *Vadas and Crowley* [2010]. Further, it is interesting to note that the distribution of LSWS zonal wavelengths observed in this study at both African and Asian longitudes (Figures 3a and 3b) resembles well the periodic spacing of EPBs observed by *Makela et al*. [2010] and the gravity wave spectrum measured by *Vadas and Crowley* [2010] [see *Makela et al*., 2010, Figure 2]. Using reverse ray tracing, *Vadas and Crowley* [2010] have shown that most of the gravity waves with zonal wavelengths ranging 100–300 km were secondary gravity waves excited by the dubbed thermospheric body forces due to dissipating primary gravity waves.

The observations from Figures 5 and 6 clearly suggest that the LSWS provides the necessary seed for R-T instability and EPBs will develop when these spatial structures grows to sufficient strengths (for example, say 2 TEC units). However, there were few exceptions can be seen from the Figure 5 where the EPBs were observed when the LSWS amplitudes are even smaller (for example, less than 1 TEC units). On the other hand, there was also a case when the LSWS amplitude exceeds 2 TEC units but no EPBs observed. It should be mentioned here that the LSWS amplitude on all the observed days were measured under slightly different conditions such as local time (longitude) sector, satellite path (IPP path), satellite orbital altitude due to finite temporal resolution (97.3 min) of observations, orbital precession, and low-inclination (13°) elliptical orbit of C/NOFS. Hence, a definite threshold for the LSWS amplitude cannot be established due to these inherent limitations involved in the measurement of LSWS peak-to-peak amplitude in this study.

5. Summary

A comprehensive study is carried out on the characteristics of zonal LSWS, and its relationship with EPBs using a large number of observations over Southeast Asia and African longitudinal sectors and the important results are summarized as follows. At both African and Asian longitudes, (i) the zonal LSWS are quite consistently observed around local sunset hours, (ii) these structures can be seen with detectable amplitudes from few degrees west of *E* region sunset terminator (sunlit region of ionosphere), (iii) the amplitudes of LSWS enhances from sunlit to dark region of ionosphere across the sunset terminator, (iv) the phase fronts of these zonal structures are observed to be field line aligned over a wide latitudinal belt for at least 5–6° (~500–600 km) centered on the dip equator, (v) the zonal wavelengths of LSWS found to vary from 100 to 700 km with a maximum between 200 to 500 km which is consistent with the earlier results reported in literature, (vi) EPBs were consistently observed during the days when the amplitudes of LSWS were grown to sufficient strengths at both the longitudinal sectors, and (vii) the LSWS over African sector appears to be stronger than over Asian longitudes.

Acknowledgments

This work is partially supported by Department of Science and Technology under the project GITA/DST/TWN/P-47/2013. The authors thank Kensuke Hangyo (Research Institute for Sustainable Humanosphere, Kyoto University) for help in data analysis. This work is partly supported by JSPS KAKENHI grants 22403011 and 25302007 and MEXT Strategic Funds for the Promotion of Science and Technology. One of the authors (R.T.T.) was supported by the National Science Foundation under grant ATM-0937858. The data collected in Vietnam were part of collaborations with HCMIP and HIG/VAST (Vietnam).

Alan Rodger thanks the reviewers for their assistance in evaluating this paper.

References

Aarons, J., J. P. Mullen, H. E. Whitney, and E. M. Mackenzie (1980), The dynamics of equatorial irregularity patch formation, motion and decay, *J. Geophys. Res.*, *85*, 139–149.

Abdu, M. A. (2001), Outstanding problems in the equatorial ionosphere-thermosphere electrodynamics relevant to spread F, *J. Atmos. Sol. Terr. Phys.*, *63*, 869–884.

Abdu, M. A., I. S. Batista, and J. A. Bittencourt (1981), Some characteristics of spread F at the magnetic equatorial station Fortaleza, *J. Geophys. Res.*, *86*, 6836, doi:10.1029/JA086iA08p06836.

Abdu, M. A., E. A. Kherani, I. S. Batista, E. R. de Paula, D. C. Fritts, and J. H. Sobral (2009), Gravity wave initiation of equatorial spread F/plasma bubble irregularities based on observational data from the SpreadFEx campaign, *Ann. Geophys.*, *27*, 2607–2622.

Bhattacharya, A., S. Basu, K. M. Groves, C. E. Valladares, and R. Sheehan (2001), Dynamics of equatorial F region irregularities from spaced receiver scintillation observations, *Geophys. Res. Lett.*, *28*, 119–122.

Dungey, J. W. (1956), Convective diffusion in the equatorial F-region, *J. Atmos. Sol. Terr. Phys.*, *9*, 304–310.

Eccles, J. V. (2004), Assimilation of global-scale and mesoscale electric fields from low-latitude satellites, *Radio Sci.*, *39*, RS1S09, doi:10.1029/2002RS002810.
Fejer, B. G., L. Scherliess, and E. R. de Paula (1999), Effects of the vertical plasma drift velocity on the generation and evolution of equatorial Spread-F, *J. Geophys. Res.*, *104*, 19,859–19,869.
Fukao, S., T. Yokoyama, T. Tayama, M. Yamamoto, T. Maruyama, and S. Saito (2006), Eastward traverse of equatorial plasma plumes observed with the Equatorial Atmosphere Radar in Indonesia, *Ann. Geophys.*, *24*, 1411–1418.
Haerendel, G. (1973), Theory of equatorial spread F, Report, Maxplanck-Institute for Extraterrestrial physics, Garching, Germany.
Huang, C.-S., and M. C. Kelley (1996), Nonlinear evolution of equatorial spread F:1. On the role of plasma instabilities and spatial resonance associated with gravity wave seeding, *J. Geophys. Res.*, *101*, 283–292, doi:10.1029/95JA02211.
Kelley, M. C. (1989), *The Earth's Ionosphere Plasma Physics and Electrodynamics*, Academic Press, San Diego, Calif.
Kelley, M. C. (2004), *The Earth's Ionosphere*, 2nd ed., 153 pp., Academic Press, Elsevier, Amsterdam.
Klostermeyer, J. (1978), Nonlinear investigation of the spatial resonance effect in the nighttime equatorial F region, *J. Geophys. Res.*, *83*, 3753.
Lee, C. C., J. Y. Liu, B. W. Reinisch, W. S. Chen, and F. D. Chu (2005), The effects of the pre-reversal drift, the EIA asymmetry, and magnetic activity on the equatorial spread F during solar maximum, *Ann. Geophys.*, *23*, 745–751.
Leitinger, R., G. Schmidt, and A. Tauriainen (1975), An evaluation method combining the differential Doppler measurements from two stations that enables the calculation of electron content of the ionosphere, *J. Geophys.*, *40*, 201–213.
Makela, J. J., S. L. Vadas, R. Muryanto, T. Duly, and G. Crowley (2010), Periodic spacing between consecutive equatorial plasma bubbles, *Geophys. Res. Lett.*, *37*, L14103, doi:10.1029/2010GL043968.
Maruyama, T. (1988), A diagnostic model for equatorial Spread F. 1.Model description and applications to electric field and neutral wind effects, *J. Geophys. Res.*, *93*, 14,611–14,622.
Mendillo, M., J. Baumgardner, X. Pi, and P. J. Sultan (1992), Onset conditions for equatorial Spread F, *J. Geophys. Res.*, *97*, 13,865–13,876.
Oppenheim, A. V., and R. W. Schafer (1989), Design of FIR filters by Windowing, in *Discrete-Time Signal Processing*, pp. 447–448, Prentice Hall, Englewod Cliffs, N. J.
Rama Rao, P. V. S., S. Tulasi Ram, K. Niranjan, D. Prasad, S. Gopi Krishna, and N. K. M. Lakshmi (2005), VHF and L-band scintillation characteristics over an Indian low latitude station, Waltair (17.7 N, 83.3E), *Ann. Geophys.*, *23*, 2457–2464.
Rottger, J. (1973), Wave-like structures of large-scale equatorial spread-F irregularities, *J. Atmos. Sol. Terr. Phys.*, *35*, 1195–1196, doi:10.1016/0021-9169(73)90016-0.
Singh, S., F. S. Johnson, and R. A. Power (1997), Gravity wave seeding of equatorial plasma bubbles, *J. Geophys. Res.*, *102*, 7399.
Takahashi, H., et al. (2009), Simultaneous observation of ionospheric plasma bubbles and mesospheric gravity waves during the SpreadFEx Campaign, *Ann. Geophys.*, *27*, 1477–1487.
Thampi, S. V., M. Yamamoto, R. T. Tsunoda, Y. Otsuka, T. Tsugawa, J. Uemoto, and M. Ishii (2009), First observations of large-scale wave structure and equatorial spread *F* using CERTO radio beacon on the C/NOFS satellite, *Geophys. Res. Lett.*, *36*, L18111, doi:10.1029/2009GL039887.
Thampi, S. V., R. T. Tsunoda, L. Jose, and T. K. Pant (2012), Ionogram signatures of large-scale wave structure and their relation to equatorial spread F, *J. Geophys. Res.*, *117*, A08314, doi:10.1029/2012JA017592.
Tsunoda, R. T. (1981), Time evolution and dynamics of equatorial backscatter plumes. 1. Growth phase, *J. Geophys. Res.*, *86*, 139–149.
Tsunoda, R. T. (1985), Control of the seasonal and longitudinal occurrence of equatorial scintillations by the longitudinal gradient in integrated F region Pedersen conductivity, *J. Geophys. Res.*, *90*, 447–456.
Tsunoda, R. T. (2005), On the enigma of day-to-day variability in equatorial spread *F*, *Geophys. Res. Lett.*, *32*, L08103, doi:10.1029/2005GL022512.
Tsunoda, R. T. (2008), Satellite traces: An ionogram signature for large-scale wave structure and a precursor for equatorial spread F, *Geophys. Res. Lett.*, *35*, L20110, doi:10.1029/2008GL035706.
Tsunoda, R. T. (2009), Multi-reflected echoes: Another ionogram signature of large-scale wave structure, *Geophys. Res. Lett.*, *36*, L01102, doi:10.1029/2008GL036221.
Tsunoda, R. T. (2010a), On seeding equatorial spread F during solstices, *Geophys. Res. Lett.*, *37*, L05102, doi:10.1029/2010GL042576.
Tsunoda, R. T. (2010b), On equatorial spread F: Establishing a seeding hypothesis, *J. Geophys. Res.*, *115*, A12303, doi:10.1029/2010JA015564.
Tsunoda, R. T. (2010c), On seeding equatorial spread F: Circular gravity waves, *Geophys. Res. Lett.*, *37*, L10104, doi:10.1029/2010GL043422.
Tsunoda, R. T. (2012), On seeding equatorial spread F: Parallel or transverse transport?, *J. Atmos. Sol. Terr. Phys.*, doi:10.1016/j.jastp.2012.10.016.
Tsunoda, R. T., and B. R. White (1981), On the generation and growth of equatorial backscatter plumes—1. Wave structure in the bottomside *F* layer, *J. Geophys. Res.*, *86*, 3610–3616.
Tsunoda, R. T., D. M. Bubenik, S. V. Thampi, and M. Yamamoto (2010), On large-scale wave structure and equatorial spread F without a post-sunset rise of the F layer, *Geophys. Res. Lett.*, *37*, L07105, doi:10.1029/2009GL042357.
Tsunoda, R. T., M. Yamamoto, T. Tsugawa, T. L. Hoang, S. Tulasi Ram, S. V. Thampi, H. D. Chau, and T. Nagatsuma (2011), On seeding, large-scale wave structure, equatorial spread F, and scintillations over Vietnam, *Geophys. Res. Lett.*, *38*, L20102, doi:10.1029/2011GL049173.
Tsunoda, R. T., S. V. Thampi, T. T. Nguyen, and M. Yamamoto (2013), On validating the relationship of ionogram signatures to large-scale wave structure, *J. Atmos. Sol. Terr. Phys.*, *103*, 30–35, doi:10.1016/j.jastp.2012.11.003.
Tulasi Ram, S., P. V. S. Rama Rao, K. Niranjan, D. S. V. V. D. Prasad, R. Sridharan, C. V. Devasia, and S. Ravindhran (2006), The role of post sunset vertical drifts at the equator in predicting the onset of VHF scintillations during high and low sunspot activity years, *Ann. Geophys.*, *24*, 1609–1616.
Tulasi Ram, S., M. Yamamoto, R. T. Tsunoda, and S. V. Thampi (2012), On the application of differential phase measurements to study the zonal large scale wave structure (LSWS) in the ionospheric electron content, *Radio Sci.*, *47*, RS2001, doi:10.1029/2011RS004870.
Vadas, S. L., and G. Crowley (2010), Sources of the traveling ionospheric disturbances observed by the ionospheric TIDDBIT sounder near Wallops Island on October 30, 2007, *J. Geophys. Res.*, *115*, A07324, doi:10.1029/2009JA015053.
Whalen, J. A. (2002), Dependence of equatorial bubbles and bottomside Spread F on season, magnetic activity, and E × B drift velocity during solar maximum, *J. Geophys. Res.*, *107*(A2), 1024, doi: 10.1029/2001JA000039.
Yamamoto, M. (2008), Digital beacon receiver for ionospheric TEC measurement developed with GNU radio, *Earth Planets Space*, *60*, e21–e24.